ARTICLE NO. 77-1506

Dual-Sensor Failure Identification Using Analytic Redundancy

Mukund N. Desai,* James C. Deckert,* and John J. Deyst Jr.†
The Charles Stark Draper Laboratory, Inc., Cambridge, Mass.

In this paper we present a reliable technique for failure detection and identification for dual flight control sensors aboard the F-8 digital fly-by-wire aircraft, and we discuss the successful application of the technique to identifying failures injected on test flight downlink data. The technique exploits the analytic redundancy which exists as relationships among variables being measured by dissimilar instruments, and it accommodates both modeling errors and the allowable errors on unfailed instruments. With straightforward modification the technique may be extended to provide failure monitoring of a single remaining sensor after the identified failure of its companion sensor.

Nomenclature

a = SPRT failure threshold (<0)
$\boldsymbol{a}$ = nongravitational acceleration vector
a_h = second derivative of altitude
a_x, a_y, a_z = longitudinal, lateral, and normal body axis components of aircraft nongravitational acceleration; also, accelerometer outputs after compensation for sensor distance from center of mass
b = SPRT no-failure threshold (>0)
B = DG case orientation angle
$\boldsymbol{c}$ = unit downward direction vector
$C_{y\beta}$ = sideforce coefficient for sideslip angle
$C_{y\delta r}$ = sideforce coefficient for rudder deflection
d,e = intermediate variables in altimeter analytic redundancy residual calculations
E = MSPRT projected worst-case error magnitude
g = acceleration of gravity
h = altitude
H_1, H_2 = failure and no-failure hypotheses, respectively
K_1, K_2 = filter gains
l = analytic redundancy residual window length
m = aircraft mass; with subscript, SPRT mean
M = Mach number
p = roll rate
P = probability density function
q = pitch rate
Q = dynamic pressure
r = yaw rate
S = wing area
t = time
T = FDI sample period
u = log likelihood ratio for successive samples, the test statistic for SPRT
$\tilde{u}$ = MSPRT test statistic
v = altitude rate
$\boldsymbol{v}$ = air-relative velocity vector
$\tilde{v}$ = measured longitudinal velocity component
v_s = velocity of sound
w = altitude filter residual
α = angle of attack
β = sideslip angle
γ = analytic redundancy residual
θ = Euler pitch angle
δ = directional gyro spin axis dip angle
δr = rudder deflection
ξ = inertial velocity vector of air-mass
ϕ = Euler roll angle
ψ = Euler yaw angle
ω = angular rate vector, with components p, q, and r

Superscripts

$\dot{(\ )}$ = derivative with respect to time
$\hat{(\ )}$ = estimate
$(\ )'$ = before measurement incorporation
$\bar{(\ )}$ = average of present and previous sample
j = denotes individual instrument value

Acronyms

AK = altitude kinematics
AR = analytical redundancy
BFM = bias failure magnitude
DFBW = digital fly-by-wire
DG = directional gyro
DR = direct redundancy
ETL = elapsed time limit
FDI = failure detection and identification
MSPRT = modified sequential probability ratio test
RK = rotational kinematics
rss = root sum square
SPRT = sequential probability ratio test
TD = translational dynamics
TK = translational kinematics
VG = vertical gyro

Presented as Paper 77-1506 at the AIAA 2nd Digital Avionics System Conference, Los Angeles, Calif., Nov. 2-4, 1977; submitted May 12, 1978; revision received July 19, 1978.

Index categories: Sensor Systems; Reliability, Maintainability and Logistics Support.

*Staff Engineer, Control and Flight Dynamics Division. Member AIAA.

†Section Chief, Control and Flight Dynamics Division. Member AIAA.

I. Introduction

THE mission-critical nature of the control system for high-performance aircraft has created a need for highly reliable survivable avionics systems. Considerations such as life-cycle cost, volume, weight, and power suggest that the required level of control sensor redundancy be supplied by keeping hardware replication to a minimum, with maximum utilization of the analytic redundancy (AR) characterized by relationships among unlike elements of the system. Willsky[1]

provides an excellent survey of current AR design methods which include failure-sensitive filters[2-4] designed to enhance failure detectability, multiple hypothesis techniques[5,6] involving a bank of filters for a wide class of failure modes, jump process formulations[7,8] to detect abrupt changes in the system, and innovations-based detection systems.[9-12] None of the above techniques gives sufficient consideration to robustness in the presence of inevitable modeling errors, and the multiple hypothesis and innovations techniques appear to possess innate complexity exceeding current aircraft flight computer constraints.

In this paper we present a reliable technique, which avoids the above shortcomings, for onboard failure detection and identification (FDI) for dual flight control sensors, and review results of the application of this technique to flight data from the F-8 digital fly-by-wire (DFBW) aircraft. The flight data covered the subsonic, transonic, and supersonic phases from takeoff to touchdown, including high-rate attitude maneuvers.[13]

We have chosen to work with dual sensors to exploit the computational simplifications that result when failure detection is performed using comparison of like-sensor outputs. The resulting tehnique resembles a simplified generalized likelihood ratio[1] algorithm in which the failure time is determined by like-sensor miscompare and the failure mode is assumed to be a bias of predefined magnitude. We postulate bias failures for two major reasons. First, although detailed descriptions of actual failure modes are not available, it is felt that bias failures are likely. Second, although designed to identify bias failures, the present technique is quite robust and will identify other failures, such as ramps and scale factors, when observability is sufficiently high. This is demonstrated in results shown in Sec. IV.

II. FDI Structure

The FDI structure is dual-mode, with failure detection accomplished by direct comparison of pairs of like instruments and identification accomplished using AR via a modification of the sequential probility ratio test (SPRT).[14] This dual-mode structure results in a very low computation load in the normal situations where failures are not present, and it allows the AR tests to be made quite robust.

During the process of failure identification, the existence of dual sensors allows an instrument to be provisionally failed, i.e., removed from all but FDI-related calculations while the FDI processing continues. This tends to minimize effective (with respect to the control system) identification time without corresponding increases in false identification rates. The provisional failure identification is made using a relaxed test criterion corresponding to minimizing a Bayesian risk function with equal a priori probability of failure in either of the dual sensors.[15]

Direct Redundancy Detector

Failure detection is accomplished through a direct redundancy (DR) detector that makes threshold tests on the moving window average of the output of instrument 1 minus the output of instrument 2 for each sensor type. If the threshold is exceeded and the average is positive (negative), it follows that either instrument 1 has a positive (negative) error or instrument 2 has a negative (positive) error. The choice of the threshold for each sensor type requires some discussion of the definition of a failed instrument. For FDI purposes, it is convenient to define a failed instrument as one having an output error magnitude larger than a stipulated *bias failure magnitude* (BFM). (This definition should not obscure the fact that in practice we would like to isolate an instrument having an output error magnitude *of the order of* BFM, e.g. 0.9 BFM.) Accordingly, the BFM for each sensor type is chosen larger than the observed errors in good instruments and large enough to be identified using the available analytic redundancy.[13] Since the identification technique, described below, is very unlikly to isolate an instrument having a failure magnitude less than BFM/2, the direct redundancy threshold is chosen to avoid detecting such failure magnitudes. Our threshold choice of three-quarter BFM results in equal probabilities of not detecting a BFM bias and of detecting a BFM/2 bias, assuming no bias in the companion sensor. The direct redundancy window size for each sensor type is calculated as a function of BFM, white noise standard deviation, and stipulated probability levels (10^{-4} for this study).

The Sequential Probability Ratio Test

The SPRT, discussed in Ref. 14, makes sequential observations of the residual process γ, which in this study represents a comparison between the suspect instrument and other unfailed instrument types. (The details of the process γ from the various AR relationships are given in Sec. III.) The sample from the process γ at time t_k is called γ_k. The SPRT gathers enough information to choose between H_1, the failure hypothesis, and H_2, the no-failure hypothesis. The log likelihood ratio z_k for the kth sample is defined as

$$z_k = -\ell n \frac{P(\gamma_k | H_1)}{P(\gamma_k | H_2)} \tag{1}$$

and the log likelihood ratio of n independent samples is given by

$$u_n = -\ell n \frac{P(\gamma_1,\ldots,\gamma_n | H_1)}{P(\gamma_1,\ldots,\gamma_n | H_2)} = \sum_{k=1}^{n} z_k \tag{2}$$

For the case of the following two hypotheses,

H_1 = at time t_k, the process γ is Gaussian with mean m_k and variance σ^2

H_2 = at time t_k, the process γ is Gaussian with mean 0 and variance σ^2

the log likelihood ratio for n successive samples given by Eq. (2) becomes

$$u_n = \sum_{k=1}^{n} \frac{m_k}{\sigma^2}\left(\frac{m_k}{2} - \gamma_k\right) \tag{3}$$

Assuming that either H_1 or H_2 is true, the stipulation of acceptable incorrect classification probabilities directly yields the thresholds $a<0$ and $b>0$ and the following decision rule:

$$\begin{aligned} u_n \le a &\quad \text{accept } H_1 \\ a < u_n < b &\quad \text{take another sample} \\ b \le u_n &\quad \text{accept } H_2 \end{aligned} \tag{4}$$

If the log likelihood ratio is between the thresholds, a choice of hypothesis cannot yet be made which meets the specified incorrect classification probabilities, and another sample must be taken.

One attractive property of the SPRT is that it minimizes the average number of observations necessary to meet these probabilities. In addition, the SPRT is independent of the a priori probabilities of the two hypotheses, and its performance in the presence of a mean or variance other than that hypothesized is readily analyzed. It is because of its inherent simplicity as shown in Eqs. (3) and (4) that the SPRT was chosen as the basic identification tool for this study.

Modification of the SPRT

There are two difficulties associated with the direct implementation of the SPRTs for the F-8 problem. First, the SPRT as described above is open-ended. Because there are

many situations in which failure observability in the AR tests can be enhanced by pilot action, we define an elapsed time limit (ETL) for each instrument type as the maximum length of time a failure of the order of BFM should require to be identified in the absence of maneuvering. If this ETL is exceeded, an unidentifiable failure is declared, and the FDI tests are reinitialized. This allows the pilot to intervene to enhance observability where possible. Selection of ETL values is discussed in detail in Ref. 13.

The second difficulty centers on the possible presence of modeling errors and allowable unfailed sensor errors in the AR residual process γ which could cause incorrect identification via the SPRT given by Eqs. (3) and (4). In order to avoid false identification based on errors in the AR residual calculations, which will be discussed in Sec. III, the following modifications to the SPRT are made:

1) The test statistic is modified from its form in Eq. (3). Assuming the identification process begins at time t_1, the modified test statistic at time t_n is defined as

$$\tilde{u}_n^j \equiv \sum_{k=1}^{n} \left[\frac{m_k^j}{\sigma^2} \left(\frac{m_k^j}{2} - \gamma_k^j \right) + \frac{|m_k^j|}{\sigma^2} E_k \right] \tag{5}$$

where E_k is the projected worst-case error magnitude in the AR test at time t_k, calculated as the sum of the dominant error magnitudes. In Eq. (5), we have introduced the instrument superscript j which assumes the value 1 or 2 and denotes which instrument of the suspect type is used in forming the residual process.

2) The modified decision rule is defined as follows, where instrument j has the more negative test statistic:

$t_n > \text{ETL}$	notify and reinitialize
$a < \tilde{u}_n^j < 0$	provisionally fail instrument j
$\tilde{u}_n^j > a$	take another sample
$\tilde{u}_n^j \le a$	identify instrument j failed, terminate the test

(6)

Note that Eqs. (5) and (6) in effect define an SPRT which only checks for the failure hypothesis, and the effect of the last term in Eq. (5) is equivalent to a moving threshold which is conservative by an amount equal to the contribution of the projected worst-case noise terms. Eqs. (5) and (6) define the *modified sequential probability ratio test* (MSPRT). It follows that as long as the threshold offset is conservative, the misclassification probabilities using the MSPRT are no greater than the design values which yielded the nominal thresholds.

Outline of the FDI Process

In this study we address the identification of failures in eleven dual instrument types aboard the F-8 DFBW aircraft: longitudinal accelerometer, lateral accelerometer, normal accelerometer, roll rate gyro, pitch rate gyro, yaw rate gyro, vertical gyro, directional gyro, barometric altimeter, Mach meter, and alpha vane. Additionally, we utilize the output of the single available beta vane for failure identification in some of the AR tests. (Some comments on failure identification for single instruments are made in Sec. V.) Each vertical gyro (VG) gives an indication of roll angle ϕ and pitch angle θ, and the failures of the indication of ϕ and θ for a single instrument are assumed to be independent, although in practice the failure of one channel results in failing the unit. The output of each directional gyro (DG) is compensated for the dynamic effect called turn error so that the change in compensated output from one sample to another is equal to the change in azimuth reference.

Four types of analytic redundancy are utilized by the algorithm: rotational kinematics (RK), altitude kinematics (AK), translational kinematics (TK), and translational dynamics (TD). Following a *redundancy trigger,* indicating the detection of the failure of one of a pair of sensors, the calculation of one MSPRT for each sensor of the suspect type for each applicable form of AR relationship is initiated. Presently only one AR relationship is employed for each sensor type except the lateral and normal accelerometers, which employ two. The mean of the MSPRT for each instrument is chosen as the BFM-sized failure signature with sign consistent with the sign information from the detector. The details of the AR MSPRT calculations are given in Sec. III.

In addition to the MSPRT's, a direct redundancy SPRT is initiated following the redundancy trigger, with the mean m_k defined to have BFM magnitude and the sign given by the detector, and the residual process γ_k defined to be the output of instrument 1 minus the output of instrument 2. If the log likelihood ratio u for this test ever becomes greater than b, a false alarm is declared, all AR identification tests are terminated, the redundancy trigger is removed, and the detection process is reinitiated.

III. Analytic Redundancy MSPRT's

Rotational Kinematics (RK)

RK is used for the identification of failures in the rate gyros and attitude gyros. The rate gyros provide noisy measurements of the aircraft body rates p, q, and r about the aircraft longitudinal, lateral, and normal (x, y, and z) axes, respectively, while the attitude gyros give noisy measurements of the Euler angles as mentioned earlier. The body rates are related to the Euler angles and their rates via

$$\begin{aligned} p &= \dot{\phi} - \dot{\psi} \sin\theta \\ q &= \dot{\theta} \cos\phi + \dot{\psi} \cos\theta \sin\phi \\ r &= -\dot{\theta} \sin\phi + \dot{\psi} \cos\theta \cos\phi \end{aligned} \tag{7}$$

We will now illustrate the use of Eqs. (7) in forming the residual process γ for the rate gyros, using the roll rate gyros as an example. Assume that a redundancy trigger is given for the roll rate gyros at time t_1. Then the residual γ_k^j for roll rate gyro j at time t_k, $k \ge 1$, is defined as

$$\gamma_k^j = \sum_{i=1}^{k} \{ \bar{p}_i^j T - [\phi_i - \phi_{i-1}) - (\psi_i - \psi_{i-1}) \sin\bar{\theta}_i^j] \} \tag{8}$$

where T is the sample period, ϕ_i is the measurement of roll angle at time t_i, ψ_i is the compensated DG output at t_i, and $\bar{p}_i^j$ and $\bar{\theta}_i^j$ are the averages of the output of roll rate gyro j and the pitch attitude measurements at t_i and t_{i-1}. Additionally, the attitude measurements are the average from two sensors if both are unfailed. The form of Eq. (8) is attractive in that it effectively avoids differentiating the noisy attitude measurements. The mean m_k^j for the MSPRT of Eq. (5) has magnitude equal to the roll rate gyro BFM times $(t_k - t_0)$. The variance σ^2 is chosen to be of the order of the roll attitude measurement variance. The worst-case error includes attitude measurement noise, 0.02 rad alignment error in both cross-axis directions, 5% scale factor error, attitude measurement bias, and error due to nonhorizontal DG spin axis. The last error in this list requires some explanation. Assuming an unfailed DG with a horizontal spin axis, the corrected azimuth angle indicated by the DG is given by[13]

$$\psi = \tan^{-1} \{ [\cos\theta \tan(\text{DG} - B) + \sin\theta \sin\phi] / \cos\phi \} \tag{9}$$

where B is a known constant indicating the orientation of the DG case with respect to the aircraft. However, if the spin axis of the DG is dipped below the horizontal by the angle δ, ψ given by Eq. (9) is in error by the amount

$$\sin^{-1} \{ \tan\delta \, (\sin\psi \sin\theta - \cos\psi \tan\phi) / \cos\theta \} \tag{10}$$

Thus, during large roll maneuvers, the residual process for the rate gyros, in particular the pitch and yaw gyros, may have substantial instantaneous error if δ is nonzero. This effect is not merely of academic interest. Extensive analysis of the test flight data discussed in Sec. IV indicates that DG 1 had a value of δ of approximately 0.13 rad. Fortunately, the FDI algorithm is able to identify this failure of DG 1 as shown in Sec. IV. However, to be conservative, we must assume some level of unidentifiable dip angle, and we currently use 0.03 rad in calculating this maneuver-dependent contribution to the total worst-case test error.

Because the rate gyro residual processes analogous to Eq. (8) are essentially unbiased at low pitch and roll attitude angles, they may be used to estimate the biases in the individual rate gyros. We are presently using first-order filters with one-minute time constants for this purpose, with the update calculations bypassed if the pitch or roll angle magnitude exceeds 0.2 rad. This estimation procedure allows a rate gyro to remain active although it contains a large, stable bias, and the instrument is declared failed only when the bias changes rapidly.

Because the sensors other than the rate gyros do not possess clean, unbiased AR relationships, they cannot easily be compensated for bias. Thus we assume biases of the order of BFM in the averaged outputs of sensors other than rate gyros used in AR residual calculations for *other* instruments. For those sensors whose failure signatures persist, i.e., the accelerometers, rate gyros, and alpha vanes, we assume that we can ultimately identify a BFM/$\sqrt{2}$ failure and use the rss value of the average of these two errors, namely BFM/2, as the worst-case bias error. For the DG's, VG's, Mach meters, and altimeters we can only identify BFM failures, and therefore we use the rss of the average of these failures, namely BFM/$\sqrt{2}$, as the worst-case bias error.

In order to use RK for identifying attitude gyro failures, the nonsingular inverse relationships to Eq. (7) are defined as follows:

$$\begin{aligned}\dot{\phi} &= p + \dot{\psi}\sin\theta \\ \dot{\theta} &= q\cos\phi - r\sin\phi \\ \dot{\psi} &= (\dot{\phi} - p)\sin\theta + (q\sin\phi + r\cos\phi)\cos\theta \end{aligned} \tag{11}$$

Attitude gyro failure identification using the RK relationships of Eqs. (11) requires the storage of a window of instantaneous residuals, with the residual process γ in Eq. (5) formed by processing the instantaneous residuals following a redundancy trigger. We will now illustrate the procedure using the indication of roll angle from the VG's as an example. Assume roll attitude DR and AR windows of length l, and denote the time of the roll attitude redundancy trigger as t_l. We define the roll attitude residual γ^j_k for VG j at time t_k, $k \geq 1$, as

$$\gamma^j_k = \sum_{i=1}^{k} \{\phi^j_i - \phi^j_{i-1} - [\bar{p}_i T + (\psi_i - \psi_{i-1})\sin\bar{\theta}_i]\} \tag{12}$$

where the term in braces is the instantaneous residual at time t_i for VG j. Equations (5) and (12) are used to calculate the MSPRT for each VG at time t_l, and the threshold tests of Eqs. (6) are applied. If necessary, a new term is added at each sample following the trigger until a decision, or ETL, is reached. Since the assumed failure mode is a bias jump in the roll attitude output from the VG, the mean m^j_k for the MSPRT has magnitude equal to the roll attitude BFM. The variance σ^2 is chosen to be of the order of the roll attitude measurement variance, and the worst-case error term E_k is composed of a step due to roll attitude measurement noise at the beginning of the window plus a ramp due to roll rate measurement bias from the beginning of the window. The $\sin\theta$ coefficient of ψ in Eq. (12) eliminates DG dip angle error from consideration in the ϕ test for most flight conditions.

We note that the same framework as used for the attitude gyros, i.e., a moving window of AR differences and an MSPRT looking for a bias jump, is also used for the Mach meters using TK and the altimeters using AK.

Altitude Kinematics (AK)

The second derivative of altitude at time t_i is given by

$$a_{h,i} = a_{x,i}\sin\theta_i - (a_{y,i}\sin\phi_i + a_{z,i}\cos\phi_i)\cos\theta_i - g \tag{13}$$

and this relationship is used to perform failure identification for the lateral accelerometers, normal accelerometers, and altimeters. A second-order discrete filter is used for each of the two altimeters. The altitude and altitude rate estimates at time t_i are $\hat{h}^j_i$ and $\hat{v}^j_i$, respectively, and the filter equations are given by

$$\begin{aligned}\hat{v}^{j'}_i &= \hat{v}^j_{i-1} + a_{h,i}T \\ \hat{h}^{j'}_i &= \hat{h}^j_{i-1} + (\hat{v}^{j'}_i + \hat{v}^j_{i-1})T/2 \\ w^j_i &= h^j_i - \hat{h}^{j'}_i \\ \hat{v}^j_i &= \hat{v}^{j'}_i + K_2 w^j_i \\ \hat{h}^j_i &= \hat{h}^{j'}_i + K_1 w^j_i \end{aligned} \tag{14}$$

In Eqs. (14), $a_{h,i}$ is computed using the averages of unfailed sensor pairs where possible, and the accelerometer outputs are compensated for their distance from the center of mass in this and all other AR equations.

The gain K_2 in Eqs. (14) is chosen to give an equivalent continuous-time filter damping coefficient of .707, while the gain K_1 is chosen to minimize the worst-case velocity estimation error in the presence of accelerometer biases and altimeter quantization as discussed in Appendix E of Ref. 13. As in the case of the attitude gyros, a moving window of filter residuals w^j is saved for each altimeter. At the time of an altimeter redundancy trigger these filter residuals are processed into $K=0$ residuals, i.e., residuals corresponding to $K_1 = K_2 = 0$ from the time of the oldest piece of data in the window. Assuming l elements in the altimeter residual window, and an altimeter redundancy trigger at time t_l, the $K=0$ residual for altimeter j at time t_k, $k \geq 1$, is given by

$$\gamma^j_k = w^j_k + d^j_{k-1} + e^j_{k-1}T \tag{15}$$

where

$$\begin{aligned} d^j_k &= d^j_{k-1} + e^j_{k-1}T + K_1 w^j_k \\ e^j_k &= e^j_{k-1} + K_2 w^j_k \\ d^j_0 &= e^j_0 = 0 \end{aligned} \tag{16}$$

Since the γ^j process defined by Eqs. (14-16) corresponds to a $K=0$ filter residual, we would expect to see a jump in this process for an altimeter with a bias failure. Thus the MSPRT mean m^j_k has magnitude equal to the altimeter BFM, and the variance is chosen of the order of the altimeter output variance. The worst-case noise term E_k is made up of initial altitude and altitude rate estimation errors plus the maneuver-dependent contributions from BFM/2 acceleration measurement biases and BFM/$\sqrt{2}$ attitude angle biases. Equations (5, 15, and 16) are used to calculate the MSPRT for each altimeter at t_l, and the threshold tests of Eqs. (6) are applied. If necessary, a new term is added at each sample following the trigger until a decision, or ETL, is reached.

In using AK to identify lateral and normal accelerometer failures, the $K=0$ filters are begun at the time of the redundancy trigger. We will illustrate this procedure for the normal accelerometers. Assume that a normal accelerometer redundancy trigger occurs at t_l. One set of $K=0$ altitude and altitude rate estimators for each normal accelerometer is

begun, with initial estimates obtained from the altimeter filters. The estimates for each accelerometer are propagated forward using Eqs. (13) and (14), but in this case $K_1 = K_2 = 0$ and the $a_{h,i}$ term is identical for both instruments *except* that $a^j_{z,i}$ is used for normal accelerometer j. The residual process γ^j_k is equal to the altitude estimate using normal accelerometer j minus the measured altitude at time t_k. In this case the MSPRT mean m^j_k is maneuver-dependent and must be calculated using Eqs. (13) and (14) assuming a BFM failure, while the variance and worst-case noise are equivalent to those enumerated for the case of altimeter failures.

Translational Kinematics (TK)

The air data sensors provide a noisy measurement of the air-relative velocity vector of the aircraft in body axes v, given by

$$v = \begin{bmatrix} \cos\beta \cos\alpha \\ \sin\beta \\ \cos\beta \sin\alpha \end{bmatrix} v_s(h) M \tag{17}$$

where β is the sideslip angle, α is the angle of attack, M is Mach number, and v_s is the speed of sound, which is a function of the altitude h. The derivative of this air-relative velocity vector is given by

$$\dot{v} = a + cg - \omega \times v - \xi \tag{18}$$

where a is the nongravitational acceleration vector, c is the unit downward direction vector, ω is the angular rate vector, and ξ is the acceleration of the air mass with respect to inertial space.

We employ TK to identify failures in the longitudinal and normal accelerometers and in the Mach meters. The use of this test for the normal accelerometers is to supplement the AK test during times of high roll angle magnitude, when the observability of normal accelerometer failures in the AK residuals is diminished. We will now illustrate the use of TK for accelerometer failure identification using the longitudinal accelerometer as an example. Following a longitudinal accelerometer trigger at time t_l, the TK residual process for longitudinal accelerometer j at time t_k, $k \geq 1$, is defined as

$$\gamma^j_k = \sum_{i=l}^{k} \left[(a^j_{x,i} - g \sin\theta_i - v_s M_i q_i \alpha_i) T - (\tilde{v}_i - \tilde{v}_{i-1}) \right] \tag{19}$$

where

$$\tilde{v}_i \equiv v_s M_i [1 - (\alpha_i)^2/2] \tag{20}$$

and the velocity of sound is updated periodically. The residual given by Eq. (19) is equivalent to a $K = 0$ filter residual for the longitudinal component of air-relative velocity, and we would expect to see a ramp in this residual for the failed accelerometer. Thus the MSPRT mean m^j_k has magnitude equal to the longitudinal accelerometer BFM times $(t_k - t_0)$.

We have chosen to cope with the uncertainty introduced by the unknown wind acceleration ξ in the following manner. First, we utilize outputs from the alpha or beta vanes to make a binary decision on the level of high-frequency turbulence—high or low. This turbulence measure is obtained by successively high-pass filtering, squaring, and then low-pass filtering TK residuals analogous to Eq. (19). We set the MSPRT variance to be 9.3 m^2/s^2 for low turbulence and 33 m^2/s^2 for high turbulence. In order to slow down the identification process to accomodate high-magnitude low-frequency wind shears, which in the short term have TK residual signatures similar to those due to failed accelerometers, we postulate a worst-case wind shear profile which is present for the first 12 s of the identification process. The magnitude of this shear is 1.5 m/s^2 for low turbulence and 3 m/s^2 for high turbulence, and its sign changes after 6 s. The worst-case noise E_k for the MSPRT includes this wind shear signature in addition to an initial velocity measurement error due to air-data noise and a 0.02 rad misalignment of the longitudinal accelerometer in the normal body axis direction.

The use of TK for Mach meter failure identification is analogous to that for the attitude gyros and altimeters. A moving window of instantaneous residuals for each Mach meter is processed following a Mach meter redundancy trigger. Assuming windows of length l and a Mach meter trigger at t_l, the MSPRT residual for Mach meter j at time t_k, $k \geq 1$, is given by

$$\gamma^j_k = \sum_{i=l}^{k} \left[\tilde{v}^j_i - \tilde{v}^j_{i-1} - (a_{x,i} - g \sin\theta_i - v_s M^j_i q_i \alpha_i) T \right] \tag{21}$$

where

$$\tilde{v}^j_i \equiv v_s M^j_i [1 - (\alpha_i)^2/2] \tag{22}$$

and the term in brackets in Eq. (21) is the instantaneous residual for Mach meter j at time t_i. In the MSPRT, the mean for Mach meter j at time t_k, m^j_k, has magnitude equal to the Mach meter BFM times $v_s[1 - (\alpha_l)^2/2]$, the high turbulence variance is used, and the worst-case noise includes an initial velocity error due to Mach meter noise and acceleration bias due to accelerometer BFM/2 bias plus wind shear.

Translational Dynamics (TD)

Translational dynamics exploits the analytic redundancy between the accelerometers and the air-data sensors via stored aerodynamic coefficient functions, and we use it as the primary test for the lateral accelerometers and the only test for the alpha vanes. For the lateral accelerometers, the MSPRT residual for instrument j at time t_k is given by

$$\gamma^j_k = a^j_{y,k} - (C_{y\beta,k}\beta_k + C_{y\delta r,k}\delta r_k) QS/m \tag{23}$$

where δr_k is the measured rudder deflection at time t_k, Q is the calculated dynamic pressure, S is the wing area, and m is the aircraft mass. The MSPRT mean has magnitude equal to the lateral accelerometer BFM, the variance σ^2 is of the order of the accelerometer noise variance, and the worst-case noise term E_k consists of 0.02 rad lateral accelerometer misalignment in the normal body axis direction, 20% error in $C_{y\beta}$, and a worst-case error from neglecting the aileron and body rate aerodynamic coefficients.

For alpha vane failure identification, the MSPRT residual for instrument j at time t_k is given by

$$\gamma^j_k = -\left[D^j_k \alpha^j_k + L^j_k (1 - (\alpha^j_k)^2/2) \right]/m - a_{z,k} \tag{24}$$

where the drag D and lift L are computed for each instrument using stored functions of alpha, Mach, and elevator position. The MSPRT mean m^j_k has magnitude equal to the residual gradient magnitude computed using the two alpha vane outputs times the alpha vane BFM. The MSPRT variance is set to 40 m^2/s^4 in high turbulence and 20 m^2/s^4 in low turbulence, and the worst-case error includes BFM/2 acceleration bias and a term reflecting aerodynamic coefficient bias.

IV. Application to Flight Test Data

In this section we discuss the application of the algorithm described in the previous section to several segments of downlink data from a test flight of the F-8 DFBW aircraft. The unfailed sensor outputs in this data are more coarsely quantized than the actual sensor outputs available to the computer for onboard FDI. For most sensor types this factor is not significant, but for the altimeters it changes the

Table 1 BFM and standard deviation levels for downlink data

Sensor	BFM	σ
a_x, m/s^2	2.0	0.3
a_y,a_z, m/s^2	1.5	0.3
p, rad/s	0.062	0.005
q,r, rad/s	0.04	0.002
ϕ, rad	0.08	0.005
θ,ψ, rad	0.037	0.003
M, M	0.045	0.003
α, rad	0.025	0.005
h, m	300	10
β, rad	. . .	0.005

quantization from 3.4 m to 30 m. This coarser quantization results in larger errors in the altitude and altitude rate estimates from the altitude filters, which lead directly to higher worst-case errors and longer identification times in the AK tests when using the downlink data.

In order to exercise fully the FDI algorithm capabilities using the downlink data, a ground rule was established that the downlink data defined an unfailed set of instruments. (This rule was relaxed in the case of DG 1 as we will discuss.) By examining the difference between like sensor outputs in the downlink data, sensor variance and minimum allowable BFM values were determined. Then a straightforward procedure, detailed in Ref. 13, was used to choose the BFM levels shown in Table 1. (The rate gyro BFM levels in Table 1 do not reflect the presence of rate gyro bias estimators, and if required these values could be lowered by a factor of three or four.)

The BFM level given for ψ in Table 1 reflects the behavior of DG 2 only, after turn error compensation of its output. As we have already mentioned, extensive analysis of the rate gyro RK residuals, using the individual DG outputs compensated for turn error assuming a horizontal spin axis, has clearly established that DG 1 is failed with a spin axis dip angle of approximately 0.13 rad. Therefore, the DG FDI parameters were chosen using only the statistics of the unfailed sensor, DG 2.

Reflecting the relaxed ground rule to account for the failure of DG 1, the final FDI design operating on this downlink data, containing no injected failures, results in no redundancy triggers for any instrument type except the DG's. The DG triggers occur during moderate roll maneuvers, and result in the identification of DG 1 as failed. This DG FDI process, using RK for failure identification, is shown in Fig. 1 for one segment of downlink data. In this figure and those that follow, four frames are shown. The first frame indicates the time history of the DR SPRT test statistic, and the second frame shows the MSPRT test statistic for each instrument. (For the sake of brevity, we will shorten the term "SPRT test statistic" to "SPRT" in the remainder of this section.) The third frame shows the AR residuals, in this case using RK, which form the inputs to the MSPRT's for the two instruments. In frames two and three, the plot marked × is associated with instrument 1 of the suspect type while the plot marked o is associated with instrument 2. The fourth frame indicates the history of an important variable relative to the AR test, in this case the roll angle ϕ in radians. The failure threshold a is chosen to be -9.2, reflecting equal misclassification probabilities of 10^{-4}. Although the downlink data is available every 20 ms, the present FDI algorithm is designed to run at 60 ms and therefore samples only every third set of downlink data. For all figures, the independent variable is time in seconds.

In the flight segment covered by Fig. 1, the aircraft is at Mach 0.63 and an altitude of 6.1 km and is trimmed for horizontal flight. At approximately 17.7 s, an aileron doublet command is initiated by the pilot, resulting in a peak roll rate magnitude of approximately 1 rad/s at 18 s. The error term in

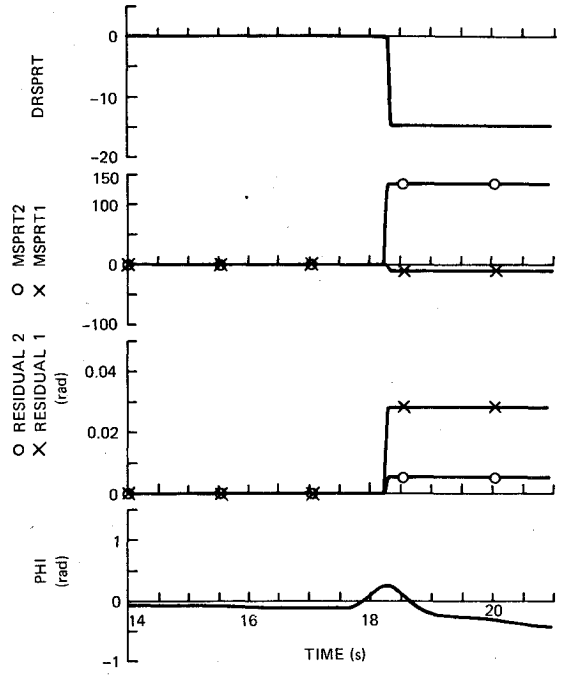

Fig. 1 Identification of DG 1 as failed.

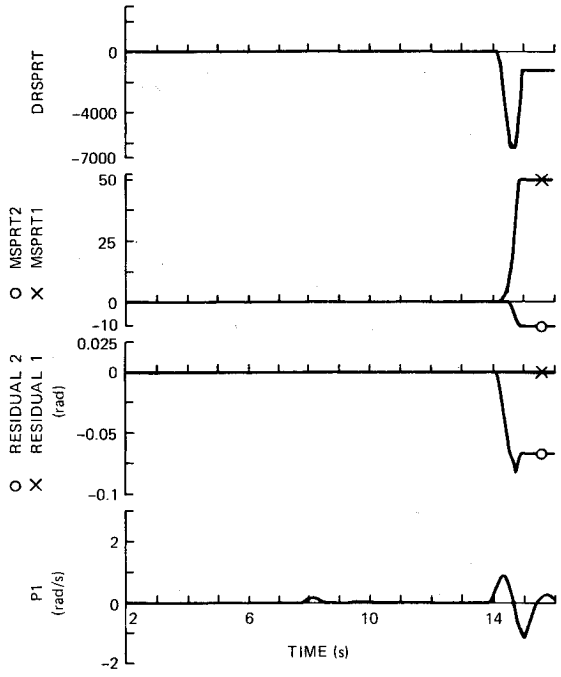

Fig. 2 Scale factor of 0.75 in roll rate gyro 2.

DG 1 arising from its dipped spin axis, which is proportional to $\tan\phi$, causes a redundancy trigger at 18.3 s, when the roll angle is approximately 0.3 rad. The DR detector indicates that the sign of the output of instrument 1 minus the output of instrument 2 is positive. This trigger initiates the directional gyro failure identification calculations. The stored window of RK residuals is processed, and based upon that information, DG 1 is identified as failed. The values of the DR SPRT, MSPRT's, and RK residuals after processing the window of residuals are shown in the figure. The large negative value of the DR SPRT corroborates the presence of the failure. Note that the large positive residual for instrument 1, shown in radians, is reflected in the negative value of its MSPRT, which is below the failure boundary, while the small positive residual for instrument 2, corresponding to the integrated

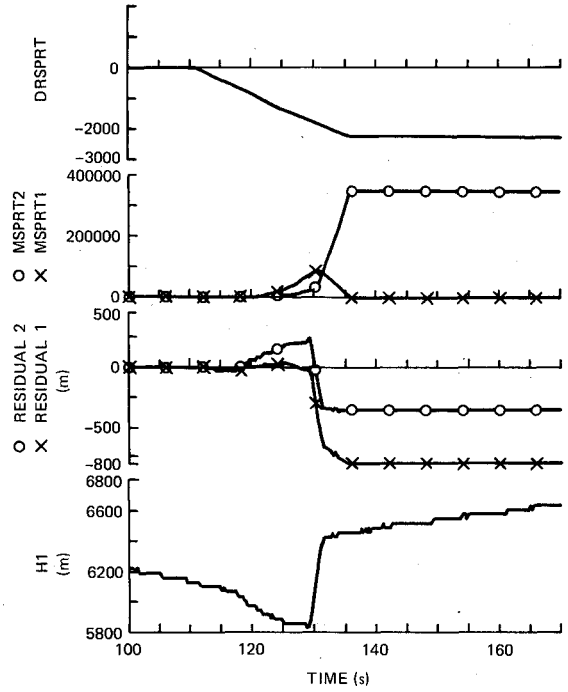

Fig. 3 1.5 m/s^2 bias in normal accelerometer 1.

effect of rate gyro errors, produces a large positive value for its MSPRT. After the identification of DG 1 as failed, the FDI calculations for the DGs are terminated, and this results in the FDI variables in the first three frames of the figure being held constant following identification.

In the remainder of this section we discuss two representative results indicating the performance of the algorithm in identifying sensor failures *injected* on the downlink data. This type of procedure is analogous to the method envisioned for onboard testing of the FDI algorithm, with an important difference being the improved quality of the sensor data available onboard. Figure 2 shows the identification of a scale factor of 0.75 in roll rate gyro 2. Figure 3 shows the identification of a bias of 1.4 m/s^2 in normal accelerometer 1 using AK.

In the test flight segment covered by Fig. 2, the aircraft is in a nearly coordinated turn at Mach 0.64, 6.4 km altitude, and a bank angle of -1.1 rad. From the beginning of this segment, the downlinked output of roll rate gyro 2 is multiplied by 0.75 before being read by the FDI algorithm, simulating a scale factor failure of that instrument. At approximately 8 s, a small aileron pulse is input by the pilot, resulting in a peak roll rate of approximately 0.2 rad/s as shown in the fourth frame, which indicates the downlinked output of roll rate gyro 1 in rad/s. This roll rate times the scale factor error in instrument 2 is not sufficiently large to result in a redundancy trigger. At approximately 13.9 s, the pilot initiates an aileron doublet command which results in a peak roll rate of approximately 1 rad/s at 14.3 s. A roll rate gyro redundancy trigger is sounded at 14.1 s, with the sign of the output of instrument 1 minus the output of instrument 2 indicated as positive. The trigger initiates the processing of RK residuals for the two roll rate gyros. We see that the RK residual for unfailed sensor 1 is essentially zero, while the residual for sensor 2, in radians, is roughly -0.25 times the integrated roll rate. The MSPRT's for the two instruments reflect this residual behavior, with the MSPRT for instrument 1 becoming quite positive and the MSPRT for instrument 2 becoming negative at 14.5 s. At this time roll rate gyro 2 is declared provisionally failed, and it would be removed from any subsequent control system calculations in an actual flight. At 14.88 s, the MSPRT for instrument 2 crosses -9.2, and roll rate gyro 2 is identified as failed. The DR SPRT immediately becomes negative following the redundancy trigger, but its slope becomes positive when the roll rate changes sign at 14.6 s. At the time the MSPRT for instrument 2 drops below -9.2, the DR SPRT is still negative, and the identification of the failure of instrument 2 is accomplished. We note that even if the DR SPRT were to have exceeded $+9.2$, roll rate gyro 2 would remain provisionally failed unless overridden by the pilot or a higher level routine.

In the flight segment covered by Fig. 3, the aircraft is at an average altitude of 6.4 km, with an initial speed of Mach 0.75. At 115 s, the engine afterburner is ignited, and at 130 s the airspeed passes above Mach 1.0. To simulate the bias failure of a normal accelerometer, a bias of 1.5 m/s^2 is added to the downlinked output of normal accelerometer 1 starting at 110 s. At 110.88 s, a redundancy trigger for the normal accelerometers is given, with a positive sign for the sensor output difference. The failure identification calculations are initiated, with the DR SPRT immediately corroborating the presence of a failure. The fourth frame in the figure shows the downlinked output of altimeter 1 in meters, while the third frame shows the normal accelerometer AK residuals, also in meters. We note that the altimeter output between 115 s and 134 s is significantly different from the true altitude of the aircraft. This error in the altimeter, as well as errors in the other air-data sensors, results from substantial alteration in the flow pattern over the vehicle at transonic speed and must not be interpreted as a malfunction of the air data sensor. We note that the AK residual for unfailed normal accelerometer 2 is approximately equal to the negative of the error in the altimeters. Simple models of these air-data sensor errors in the transonic region are added to the worst-case noise calculation for the AK MSPRT's. Thus, although the AK MSPRT for normal accelerometer 2 is looking for a positive residual, and in fact a positive residual for instrument 2 is present for many seconds, the worst-case error term in the MSPRT calculations keeps the MSPRT for instrument 2 positive. Following the large jump in the altimeter output at 130 s, the slope of the AK MSPRT for instrument 1 becomes negative, and normal accelerometer 1 is identified as failed at 135.66 s.

In this section, we have discussed the successful application of the flight control sensor FDI algorithm to flight test downlink data. Efforts were made to inject failures at the worst times, i.e., times of maximum worst-case test error, E_k. Although space limitations preclude discussion of all of the sensor failures which were simulated, the results we have presented are indicative of the robustness, reliability, and speed which characterize the algorithm. Of particular importance is the fact that the MSPRT's use of a bias failure hypothesis in no way prevents the identification of other more complex failures, as shown in Figs. 1 and 2. In addition it should be emphasized that regardless of the failure mechanism, if the failure magnitude exceeds BFM and persists, it will be identified with the stipulated probabilities for the rate gyros, accelerometers, and alpha vanes. A final important point is that the structure of the MSPRT, i.e., the addition of a worst-case error term to the failure threshold, allows simple adaptation of the algorithm to unmodeled sensor behavior (e.g., air-data sensor transonic error and acceptable rate gyro biases) without the need for elaborate modeling of the sensors themselves.

V. Additional Topics

Instrument Self-Test

One form of information which has been ignored in the discussion to this point is the physical limitation on changes in the aircraft state from one sample time to the next. By exploiting this limitation, the effect of extremely large sensor failures upon the control system may be minimized. Thus we have added to the FDI algorithm a self-test routine which provisionally fails a sensor when an abrupt change in its output persists over a three-sample interval.

FDI for Single Sensors

A straightforward adaptation of the present FDI algorithm is possible which allows failure monitoring of the single instrument of a dual pair remaining after the identification of the failure of its companion sensor. The AR relationships which have been described above are employed, and two MSPRT's for the remaining sensor are calculated at each sample, one using a positive mean and the other using a negative mean. Each MSPRT is treated independently. A time interval is chosen, significantly shorter than ETL, after which the BFM failure signature dominates the white noise in the AR process. If after that time has elaped, the SPRT portion of the MSPRT, i.e., the MSPRT with the noise term removed, is positive, the MSPRT is reset to zero and the process is repeated. Otherwise the calculations are continued until either: 1) the SPRT portion of the MSPRT becomes positive, at which time the MSPRT is reset, or 2) the MSPRT crosses the failure boundary and the instrument is identified as failed. As Chien[8] explains, the failure boundary should be lowered using this approach to obtain the same mean time between false identifications as that for a standard SPRT using two boundaries. This lowered failure boundary for our example is approximately -11.4.

If more than one instrument failure has occurred, and the AR relationship contains more than one sensor type without dual redundancy (e.g., RK with only a single roll rate gyro and a single VG), this approach cannot reliably discriminate which of the single sensors has failed. In such a situation, identification requires more elaborate techniques such as the GLR approaches described in Ref. 1.

VI. Conclusions

We have described a technique for reliable onboard detection and identification of failures in dual aircraft control system sensors, and we have enumerated straightforward modifications of the technique which allow failure monitoring of a single sensor after the identified failure of one member of the pair. Performance results using flight test data demonstrate the reliability of the technique and its robustness in the presence of several types of simulated sensor failures. The failure identification times which have been obtained for the small, BFM-sized failures are acceptably short, while reliability is guaranteed by explicitly allowing for worst-case errors, due to modeling errors and acceptable unfailed sensor errors, in the MSPRT formulation.

Acknowledgment

This work was supported by the NASA Dryden Flight Research Center through contract NAS4-2409.

References

[1]Willsky, A.S., "A Survey of Design Methods for Failure Detection in Dynamic Systems," *Automatica,* Vol. 12, Nov. 1976, pp. 601-611.

[2]Beard, R.V., "Failure Accommodation in Linear Systems through Self-Reorganization," NASA CR-118314, 1971.

[3]Jones, H.L., "Failure Detection in Linear Systems," Ph.D. dissertation, Dept. Aeronautics and Astronautics, M.I.T., Cambridge, Mass., Sept. 1973.

[4]Kerr, T.H., "A Two Ellipsoid Overlap Test for Real Time Failure Detection and Isolation by Confidence Regions," presented at the Pittsburg Conference on Modeling and Simulation, April 1974.

[5]Montgomery, R.C. and Caglayan, A.K., "Failure Accommodation in Digital Flight Control Systems by Bayesian Decision Theory," *Journal of Aircraft,* Vol. 13, Feb. 1976, pp. 69-75.

[6]Willsky, A.S., Deyst, J.J., and Crawford, B.S., "Two Self-Test Methods Applied to an Inertial System Problem," *Journal of Spacecraft and Rockets,* Vol. 12, July 1975, pp. 434-437.

[7]Davis, M.H.A., "The Application of Nonlinear Filtering to Fault Detection in Linear Systems," *IEEE Transactions on Automatic Control,* Vol. AC-20, April 1975, pp. 257-259.

[8]Chien, T.T., "An Adaptive Technique for a Redundant Sensor Navigation System," NASA CR-140313, 1972.

[9]Mehra, R.K. and Peschon, J., "An Innovations Approach to Fault Detection and Diagnosis in Dynamic Systems," *Automatica,* Vol. 7, Sept. 1971, pp. 637-640.

[10]Willsky, A.S. and Jones, H.L., "A Generalized Likelihood Ratio Approach to the Detection and Estimation of Jumps in Linear Systems," *IEEE Transactions on Automatic Control,* Vol. AC-21, Feb. 1976, pp. 108-112.

[11]Deyst, J.J. and Deckert, J.C., "Maximum Likelihood Failure Detection Techniques Applied to the Shuttle RCS Jets," *Journal of Spacecraft and Rockets,* Vol. 13, Feb. 1976, pp. 65-74.

[12]Cunningham, T., Carlson, D., Hendrick, R., Shaner, D., Hartmann, G., and Stein, G., "Fault Tolerant Digital Flight Control with Analytical Redundancy," AFFDL-TR-77-25, May 1977.

[13]Deckert, J.C., Desai, M.N., Deyst, J.J. and Willsky, A.S., "Reliable Dual-Redundant Sensor Failure Detection and Identification for the NASA F-8 DFBW Aircraft," The Charles Stark Draper Lab., Inc., Cambridge, Mass., R-1077, May 1977; also NASA CR-2944, Feb. 1978.

[14]Wald, A., *Sequential Analysis,* Dover, New York, 1973, Chap. 3.

[15]Van Trees, H.L., *Detection, Estimation, and Modulation Theory,* Part 1, Wiley, New York, 1968, pp. 24-26.